AGU PUBLICATIONS

Tectonics

RESEARCH ARTICLE
10.1002/2014TC003660

Key Points:
- Two major thrust emplacement stages triggered the Zagros Foreland basins
- Variations of the elastic thickness controlled foreland basins geometries
- An extra load is required to explain ~20% of the current Arabian plate flexure

Supporting Information:
- Readme
- Movie S1

Correspondence to:
E. Saura,
esaura@ictja.csic.es

Citation:
Saura, E., D. Garcia-Castellanos, E. Casciello, V. Parravano, A. Urruela, and J. Vergés (2015), Modeling the flexural evolution of the Amiran and Mesopotamian foreland basins of NW Zagros (Iran-Iraq), *Tectonics*, *34*, 377–395, doi:10.1002/2014TC003660.

Received 19 JUN 2014
Accepted 26 JAN 2015
Accepted article online 30 JAN 2015
Published online 11 MAR 2015

Modeling the flexural evolution of the Amiran and Mesopotamian foreland basins of NW Zagros (Iran-Iraq)

Eduard Saura[1], Daniel Garcia-Castellanos[1], Emilio Casciello[1], Vanessa Parravano[1], Aritz Urruela[1], and Jaume Vergés[1]

[1]Group of Dynamics of the Lithosphere, Institute of Earth Sciences Jaume Almera, CSIC, Barcelona, Spain

Abstract The evolution of the Amiran and Mesopotamian flexural basins of the Zagros belt is approached by coupled 2-D forward modeling of orogenic wedge formation, lithospheric flexural isostasy, and stream power erosion/transport/sedimentation. Thrust geometries and sequence of emplacement derived from geometric and kinematic models presented here are the inputs to our evolutionary model, constrained by basin geometry, sediment volume, and topography. Modeling results confirm that the Zagros flexural basins evolution is consistent with two stages of deformation: (1) the obduction stage involving the Kermanshah accretionary complex and a basement unit and (2) the collision stage, emplacing the Gaveh Rud and Sanandaj-Sirjan domains in the hinterland and forming a basement duplex in the outer part. Results provide quantitative insights into processes involved in mountain and basin building. The lithospheric equivalent elastic thickness (*Te*) changed from 20 km during the Amiran stage (~90–50 Ma) to 55 km during the Mesopotamian subsidence stage (last 20 Myr). The Amiran basin results from flexure of the Arabian plate below the load of the Kermanshah cover and basement thrust sheets. During this stage, material eroded in the inner parts was enough to fill the flexural trough. The Mesopotamian basin formed in front of the outermost basement units flexing the Arabian plate. During this latter stage, material eroded from the orogenic wedge was not enough to fill the Mesopotamian basin. An additional longitudinal sediment supply of up to 200 m/Myr is required to fill the flexural basin.

1. Introduction

The long-term convergence between Arabia and Eurasia resulted in the closure of the more than 1500 km wide Neo-Tethys Ocean from Late Jurassic to Recent [e.g., *Stöcklin*, 1968; *Berberian and King*, 1981; *Stampfli and Borel*, 2002; *Golonka*, 2004; *Barrier and Vrielynck*, 2008; *McQuarrie and Van Hinsbergen*, 2013]. The closure of the Neo-Tethys was controlled by the structure of the NE margin of the Arabian plate, the large-scale dynamics of the NE dipping oceanic subduction beneath Eurasia, the obduction of oceanic lithosphere close to Arabia, and the collision of small continental and volcanic arc domains (Iranian blocks) of the SW margin of Eurasia. A significant part of this geological history is preserved in the thin-skinned thrust system (Imbricated Zone) and the flexural basins that run parallel to the suture zone in the internal Zagros orogenic system, from Turkey and Iraq, in the NW, to Iran and Oman in the SE (Figure 1).

The Arabian passive margin originated from the opening of the Neo-Tethys Ocean during Late Paleozoic to Early Triassic rifting and underwent stable and subsiding conditions during most of the Mesozoic [*Berberian and King*, 1981; *Talbot and Alavi*, 1996; *Stampfli and Borel*, 2002]. During Late Jurassic to Early Cretaceous time, the Eurasian and Arabian plates began to converge and the Neo-Tethys Ocean started subducting under Eurasia [*Stampfli and Borel*, 2002; *Golonka*, 2004]. However, the thick Mesozoic sedimentary succession on the NE margin of the Arabian plate did not record the transition from passive to active settings until around the early Late Cretaceous [e.g., *Braud*, 1987; *Sengor*, 1990; *Piryaei et al*., 2010]. This major contractional event manifested as obduction of a large segment of Neo-Tethys oceanic crustal domain onto the Arabian margin. During this process, the Arabian plate flexed down, forming the Tanjero-Kolosh flexural basin, in Kirkuk embayment in Kurdistan [*James and Wynd*, 1965; *Jassim and Goff*, 2006; *Karim et al*., 2011; *Lawa et al*., 2013], the Amiran foreland basin in Lurestan, mostly preserved across the folded cover succession [e.g., *James and Wynd*, 1965; *Homke et al*., 2009; *Saura et al*., 2011], the Gurpi-Pabdeh foreland basin in Fars [*Motiei*, 1993; *Hessami et al*., 2001; *Piryaei et al*., 2010], and the Aruma foreland basin in Oman [*Glennie et al*., 1974; *Searle et al*., 1987; *Nolan et al*., 1990]. During this period, the major Neo-Tethys subduction front was located at a

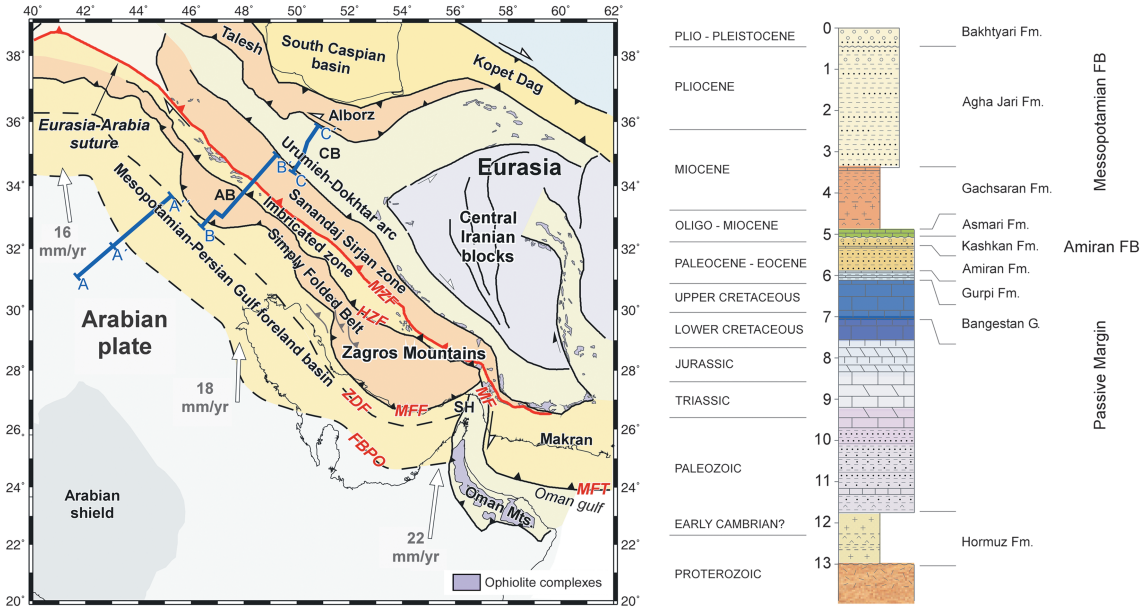

Figure 1. Structural map of the Eurasia-Arabia collision zone including the main units of the area and the location of the studied transect: Pink line—*Vergés et al.* [2011b]; Blue line—*Aqrawi et al.* [2010]. AB—Amiran foreland basin; CB—Central basin; MZF—Main Zagros Fault; HZF—High Zagros Fault; MF—Minab Fault; MFF—Mountain Front Fault; MFT—Makran frontal thrust; ZDF—Zagros deformation front; FBPO: Foreland basin pinch out, based on *Fouad* [2010] and *Hessami et al.* [2001]. Modified after *Jiménez-Munt et al.* [2012]. In the right-hand side a synthetic stratigraphic column of the Zagros Mountains is presented [modified after *Vergés et al.*, 2011a].

distance of about 1500 km to the East [*McQuarrie et al.*, 2003]. Subsequently, ongoing Arabia-Eurasia convergence led to the final oceanic closure and continental collision from late Oligocene to early Miocene [*Stoneley*, 1981; *Agard et al.*, 2005; *Horton et al.*, 2008; *Mouthereau et al.*, 2012]. This collision resulted in a major lithospheric flexure of the Arabian plate and the onset of deposition in the Mesopotamian foreland basin. Arabia-Eurasia convergence and associated deformation and deposition continued during Miocene and Pliocene times [*Homke et al.*, 2004; *Khadivi et al.*, 2010; *Ruh et al.*, 2014] to reach the current configuration of the Zagros fold belt.

The Amiran and Mesopotamian foreland basins, in the Lurestan area, both resulting in the thickening of the Zagros orogeny, display significantly divergent geometric and depositional characteristics despite their partial geographic overlap. This suggests a different behavior of the Arabian plate and the depositional system during their evolution and thus of the interplay between surface and deep processes. Since these basins are subsequently related to the obduction and collision stages, an accurate characterization of these features and their relationship with their source areas will give insights into the geodynamic evolution, shortening, and timing of the deformation of the Zagros Mountains and the preorogenic geometry of the Arabian margin in the Lurestan area.

The aims of this paper are threefold: (i) to determine the kinematic evolution of the fold system of the Zagros using published crustal balanced sections [*Vergés et al.*, 2011b] and a kinematic model to obtain the best fit of existing data on basin evolution; (ii) to quantitatively ascertain the variation of the mechanical rigidity (elastic thickness) of the different domains of the Arabian plate; and (iii) to study the coupled evolution of tectonics and surface processes that controlled the sedimentary fill of both the Late Cretaceous to Eocene Amiran and Miocene to Pliocene Mesopotamian foreland basins through time. To achieve these goals, the evolution of the Amiran and Mesopotamian foreland basins is studied, along a ~700 km long transect in NW Zagros constrained by field, seismic, and published data [*Aqrawi et al.*, 2010; *Vergés et al.*, 2011b] (Figure 2). We use the geometry of the Amiran and Mesopotamian foreland basins constrained from field and seismic data [*Mohammed*, 2006; *Aqrawi et al.*, 2010; *Saura et al.*, 2011] to estimate the elastic thickness of the lithosphere from the bending of the Arabian plate along the study transect. A 2-D dynamic approach is then designed to quantitatively link the topographic, tectonic, and sedimentary evolution of the system and used to constrain potential crustal and subcrustal loads needed to account for the flexure of the Amiran and Mesopotamian stages. The presented modeling provides a nonunique but consistent and quantitative reconstruction of the progressive involvement

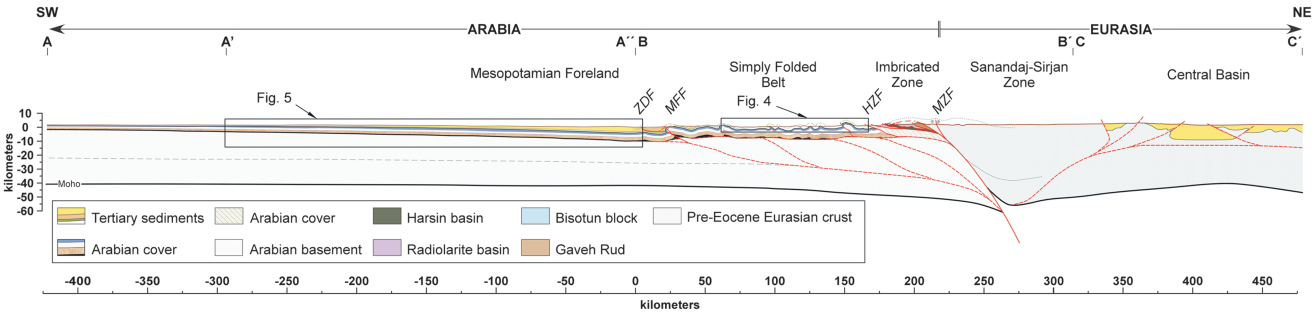

Figure 2. Crustal cross section across the Eurasia-Arabia suture zone from the Alborz Mountains to the undeformed Arabian plate, modified after *Morley et al.* [2009], *Aqrawi et al.* [2010], and *Vergés et al.* [2011b]. Location in Figure 1. MZF—Main Zagros Fault; HZF—High Zagros Fault; MFF—Mountain Front Fault; ZDF—Zagros deformation front.

of the NE Arabia margin in the Zagros Alpine collision, which is useful for the geodynamic understanding of the Zagros orogenic belt and its foreland basin development.

2. Tectonic Structure and Evolution of NW Zagros Mountains

The NW Zagros Mountains include, from NE to SW, (i) the Sanandaj-Sirjan metamorphic Zone, in the Eurasian plate, (ii) the accreted thrust sheets of the Imbricated Zone, (iii) the decoupled cover and basement of the Simply Folded Belt, and (iv) the Mesopotamian foreland basin in the Arabian plate (Figures 1 and 2). The studied transect runs from the southern front of the Alborz Mountains to the undeformed Arabian plate, across the Lurestan arc (Figure 1). In this transect, the Imbricated zone is defined by the Kermanshah complex, and the detached cover of the Simply Folded Belt corresponds to the Lurestan arc, also involving the Amiran foreland basin. The crustal structure of this area is defined by a thickened crust underneath the suture area (~60 km) [*Paul et al.*, 2010], resulting from the overthrusting of the Sanandaj-Sirjan thrust stack on top of the NE border of the downflexed Arabian plate. SW of the Eurasia-Arabia suture, defined in this area by the Main Zagros Fault (MZF; Figure 2), a duplex system involving the middle crust underlies the Imbricated Zone and the Simply Folded Belt [*Blanc et al.*, 2003; *McQuarrie*, 2004; *Alavi*, 2007; *Vergés et al.*, 2011b], which are separated by the High Zagros Fault (Figure 2). Basement involvement in the thrust system (Figures 2 and 4) is observed elsewhere in the Zagros as inferred from seismotectonic [e.g., *Berberian*, 1995; *Talebian and Jackson*, 2004; *Tatar et al.*, 2004], modeling [e.g., *Mouthereau et al.*, 2006] and structural points of view [e.g., *Molinaro et al.*, 2004; *Sherkati and Letouzey*, 2004; *Molinaro et al.*, 2005; *Mouthereau et al.*, 2007]. The Zagros deformation front is buried within the Mesopotamian foreland basin, beyond the Mountain Front Fault, a kilometer-scale structural step delineating the SW border of the Simply Folded Belt [*Emami et al.*, 2010]. Along the SW boundary of the Mesopotamian foreland basin, Mesozoic and Paleozoic sediments are exposed in the Arabian plate, with average altitudes of about 550 m. Crustal thicknesses of the Arabian plate calculated in this area range between ~35 and ~41 km [*Gök et al.*, 2008; *Jiménez-Munt et al.*, 2012]. *Vergés et al.* [2011b] estimated a minimum shortening of 180 km with an average shortening rate of $\sim 2\ \mathrm{mm\ yr^{-1}}$ for the last 90 Myr, based on the restored geometry of the NE Arabian plate, including from SW to NE, six different tectonosedimentary domains: the Cretaceous Lurestan margin, the Radiolarite basin, the Harsin basin, the Bisotun platform, the Neo-Tethys, the Gaveh Rud volcanic arc, and the Sanandaj-Sirjan zone. However, there is controversy on the original position of the Harsin basin, with respect to the Radiolarite basin and the Bisotun platform. These units are currently stacked in the Imbricated Zone, and their restoration is not straightforward [*Braud*, 1987]. Traditionally accepted models interpret the serpentinized rocks of the Harsin basin as ophiolites of the Neo-Tethys domain, originally located NE of the Bisotun platform [*Braud*, 1987; *Agard et al.*, 2005]. Furthermore, recent studies interpret the Harsin basin structure as a highly extended basin, exposing serpentinized peridotites that separated the Radiolarite basin from the Bisotun continental block before the Cenomanian [*Wrobel-Daveau et al.*, 2010].

Regional apatite fission track studies have evidenced the occurrence of several cooling/denudation events in the inner zones of the Zagros [*Homke et al.*, 2010; *Gavillot et al.*, 2010; *Khadivi et al.*, 2012] (Figure 3). In the study area, *Homke et al.* [2010] identify five main stages occurring during the pre-Middle Jurassic (~171, ~225 Ma);

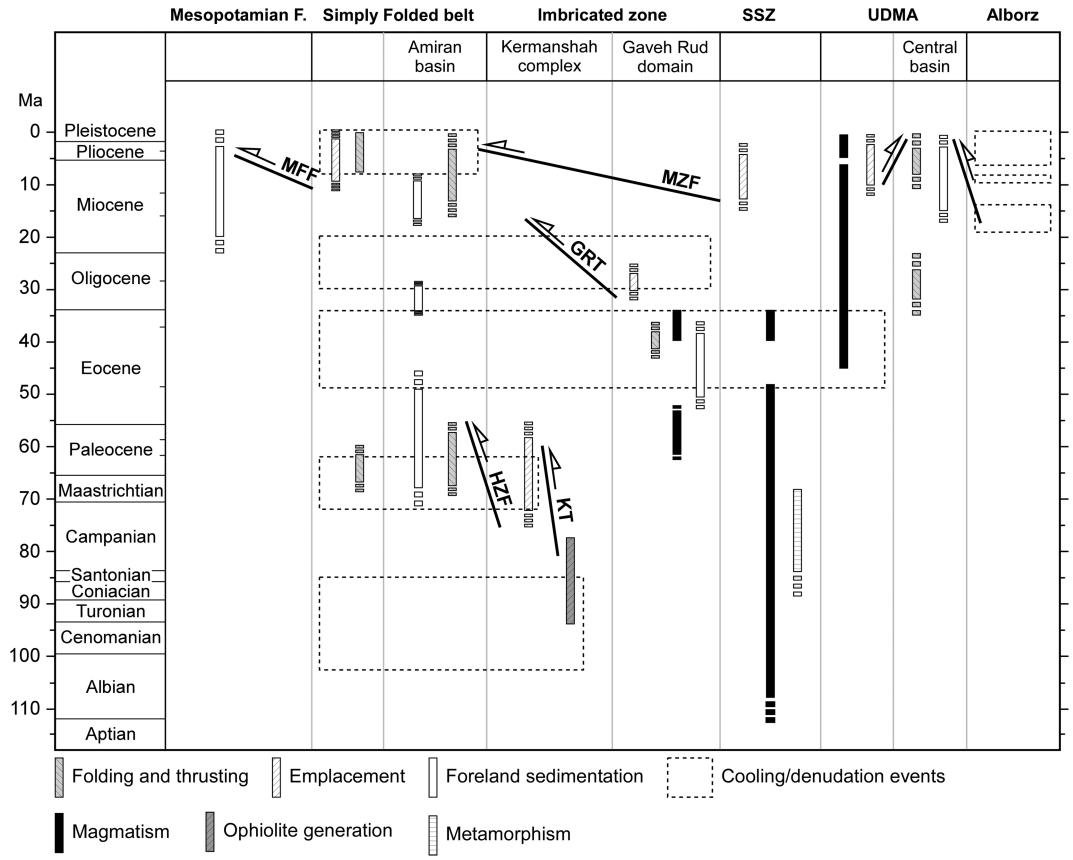

Figure 3. Compilation of the main sedimentary, tectonic, and magmatic events in the geodynamic evolution of the NW Zagros orogen. MZF—Main Zagros Fault; GRT—Gaveh Rud thrust; KT—Kermanshah thrust; HZF—High Zagros Fault; MFF—Mountain Front Fault. Compiled after *Ballato et al.* [2008], *Morley et al.* [2009], *Homke et al.* [2010], and *Ballato et al.* [2013].

early Late Cretaceous (~91 Ma); Late Cretaceous to Early Paleocene (~66 Ma); middle to Late Eocene (~38 Ma); and Late Oligocene to Early Miocene (~22 Ma). The oldest cooling ages, obtained from clasts from the Zagros foreland basins, most probably record cooling events in the source area, in the obduction complex, which are to be related to preorogenic processes such as the opening of the Neo-Tethys [*Stöcklin*, 1968; *Stampfli and Borel*, 2002], the exhumation of the mantle beneath the Harsin basin [*Wrobel-Daveau et al.*, 2010], or ophiolite generation in the distal Arabian margin [*Delaloye and Desmons*, 1980; *Saccani et al.*, 2013]. A similar scenario was described in the Fars area by *Khadivi et al.* [2012], where Jurassic to Early Cretaceous cooling ages in detrital grains of the foreland basin can be correlated with cooling ages in the obduction complex [*Babaie et al.*, 2006] which is the source area. The Late Cretaceous to Early Paleocene event can be correlated with the stacking of thrust sheets on top of the Arabian margin during the obduction stage [*Agard et al.*, 2005], leading to the creation of the Amiran basin. The Middle to Late Eocene event corresponds to a protracted period of quiescence with very slow or nondeposition in the Zagros foreland. Besides, compression and associated uplift shifted toward the NE, along the front of the Sanandaj-Sirjan domain and associated Gaveh Rud forearc basin [*Homke et al.*, 2010]. The Oligocene to Early Miocene cooling phase roughly coincides with the onset of the second major phase of flexure [*Agard et al.*, 2005; *Horton et al.*, 2008]. This new period can be correlated with the collision stage, whose onset has been dated between 35 Ma and 20 Ma [*Mouthereau et al.*, 2007; *Gavillot et al.*, 2010; *Agard et al.*, 2011; *Khadivi et al.*, 2012; *McQuarrie and Van Hinsbergen*, 2013]. During the Miocene and Pliocene, deformation propagated toward the foreland across the Simply Folded Belt [*Homke et al.*, 2004; *Emami*, 2008; *Fakhari et al.*, 2008; *Khadivi et al.*, 2010]. Coevally, in the hinterland, the Urumieh-Dokhtar arc is emplaced northeastward on top of the Central Basin [*Morley et al.*, 2009], which is also overthrusted in the north by the Alborz Mountains system [*Ballato et al.*, 2008, 2013] (Figure 3). After this stage, the Zagros Fold Belt reached its current configuration, as did the different domains located between the stable Arabian and Eurasian blocks.

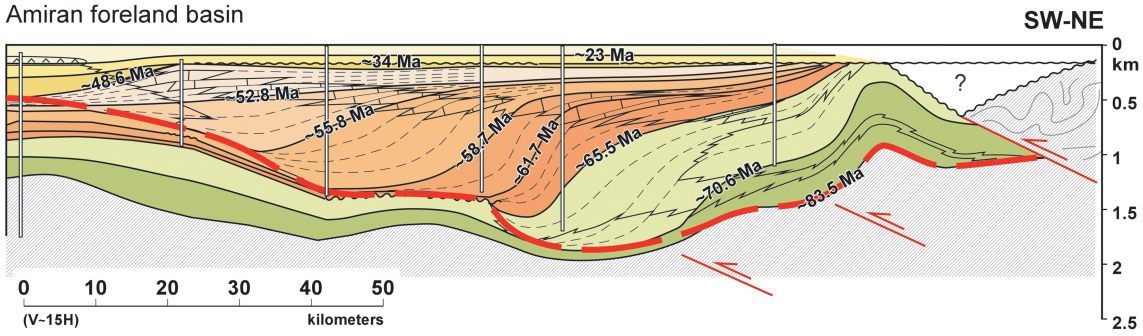

Figure 4. Architecture of the Amiran foreland basin before collision, after *Saura et al*. [2011]; see location in Figure 2. Red, dashed line corresponds to the base of the foreland basin, which is used as a modeling constraint. The location of field stratigraphic sections used to constrain this reconstruction is indicated. The basin infill is characterized by a diachronous, southwestward migrating, shallowing upward, mixed clastic-carbonate succession. From internal to external areas, time lines cross the formation boundaries, passing from continental Kashkan red beds to Taleh Zang mixed clastic-carbonate platforms, Amiran slope deposits and to basinal Gurpi-Pabdeh shales and marls. Vertical white polygons indicate the location of measured and dated stratigraphic sections [*Saura et al*., 2011].

2.1. The Amiran Foreland Basin

The Late Cretaceous to Eocene obduction stage resulted in the accretion of the Imbricated Zone over the Arabian margin associated with the formation of the Amiran foreland basin (Figure 1). The Amiran foreland basin is located within the Simply Folded Belt, between the High Zagros Fault and the Kabir Kuh anticline in the Lurestan area (Figures 2 and 4) and probably extended northwestward into the Tanjero-Kolosh foreland basin in the Kirkuk embayment in Kurdistan (Iraq) [*James and Wynd*, 1965; *Jassim and Goff*, 2006], as suggested by angular unconformities observed in this area [*Karim et al*., 2011; *Lawa et al*., 2013]. Toward the southeast, the early Eocene succession of the Fars area is characterized by marine and marine continental transitional deposits, shallower than the Amiran basin flysch deposits (Jahrum and Sachun formations) [*James and Wynd*, 1965]. A similar foreland basin evolution is envisaged in the Oman area, developing ahead of the obducted Oman ophiolite [e.g., *Alsharhan*, 1989; *Robertson et al*., 1990; *Warburton et al*., 1990].

Although the Amiran basin is currently deformed, recently published isopach maps [*Casciello et al*., 2009; *Farzipour-Saein et al*., 2009; *Saura et al*., 2013] and accurate dating of the basin fill [*Saura et al*., 2011] enable the reconstruction of the basin geometry during the emplacement of the obduction complex (Figure 4). The basin fill is characterized by a diachronous, shallowing upward, mixed clastic-carbonate succession that was deposited from Late Cretaceous to early Eocene, while prograding southwestward at an average rate of ~5 mm yr^{-1} [*Saura et al*., 2011]. After the emplacement of the obduction complex, the Amiran basin had a width of 145 km and a maximum thickness of 2 km at the center of the basin, approximately. Consequently, the basin wedges out toward the SW and NE, where a structural uplift of about 1.3 km has been estimated [*Homke et al*., 2009] (Figure 4).

2.2. The Mesopotamian Foreland Basin

The Mesopotamian foreland basin and its southeastern continuation along the Persian Gulf developed in front of the Zagros fold belt during the collision stage. The most proximal part of the foreland basin is characterized by NW-SE Zagros trending anticlines buried beneath the large alluvial plains of Iraq and Iran [e.g., *Dunnington*, 1968; *Mohammed*, 2006]. The Zagros deformation front separates these Zagros folds from roughly N-S oriented large inverted folds that dominate the Persian Gulf and the Abadan plains [e.g., *James and Wynd*, 1965; *Alavi*, 2004; *Abdollahie Fard et al*., 2006; *Vergés et al*., 2011a].

The Mesopotamian foreland basin extends along the Zagros Mountains front and continues into the Persian Gulf with a total length of almost 2000 km (Figure 1). The Mesopotamian foreland basin developed ahead of the growing Zagros fold belt by the down flexure of the Arabian plate, during and after the Arabia-Iran continental collision [e.g., *McQuarrie et al*., 2003; *Agard et al*., 2011; *Mouthereau et al*., 2012; *McQuarrie and Van Hinsbergen*, 2013]. The width of the basin is very variable, as a consequence of the sinuous trace of the Mountain Front Fault. Its maximum width is ~375 km, in the Dezful Embayment, whereas the minimum width is ~150 km, NW of Qatar Peninsula [*Hessami et al*., 2001] (Figure 1). In the study transect, the Mesopotamian foreland basin is ~300 km wide and is filled by about 5 km of sediments [*Aqrawi et al*., 2010] (Figure 5).

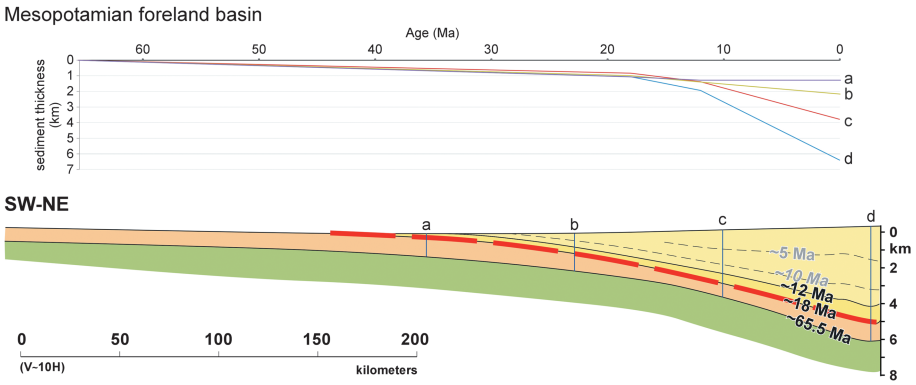

Figure 5. Architecture of the Mesopotamian foreland basin based on a megaseismic transect [modified after *Aqrawi et al.*, 2010]. Age attribution based on *Mohammed* [2006]. Red, dashed line corresponds to the base of foreland basin used as a modeling constraint. See location in Figure 2.

The Neogene basin infill (Lower and Upper Fars formations) is mostly nonmarine within the Mesopotamian foreland, grading into transitional and shallow water deposits in the Persian Gulf (with present maximum water depths of around 90 m). The age and geometry of the basin fill, based on horizon attribution in a megaseismic profile across the Mesopotamian foreland basin [*Mohammed*, 2006], shows that basin flexure started at around 18 Ma and accelerated after 12 Ma. These values are in agreement with the ages of the onset of collision-related folding in the Simply Folded Belt, based on magnetostratigraphic and biostratigraphic studies [*Homke et al.*, 2004; *Emami*, 2008; *Fakhari et al.*, 2008; *Khadivi et al.*, 2010] (Figure 3).

3. Kinematic Model: Sequence of Deformation

A forward kinematic model has been chosen, in order to quantify and obtain the thrust system parameters, geometry, displacement, and sequence of emplacement required to constrain the geodynamic modeling. We use a kinematic forward model based on the fault-parallel flow algorithm (2DMove, Midland Valley Exploration, Scotland) (Figure 6). This model does not include erosion and sedimentation, nor model isostasy. As a consequence, the obtained model entails some dynamic inconsistencies (i.e., exaggerated topographic values). However, the crustal thickness in the final model, measured from the base of the crust (unflexed) to the current erosion level, is 50 km which is comparable to the same measure in the balanced cross section. The best fit with the geological cross section was achieved with four basement units in the Arabian margin, which allowed a more homogeneous thickening of the whole Arabian crust and emplacement of the basement of the Bisotun block together with the Harsin and Radiolarite basins. The resulting sequence is described below.

The initial modeling stages correspond to Campanian-Maastrichtian times when the cover units of the Kermanshah complex imbricated (Figure 6b), resulting in a shortening of 145 km. This value, which can be assumed to correspond to obduction overlap, is slightly below 180 km of overlap as proposed by *McQuarrie and Van Hinsbergen* [2013], who extrapolated their estimation from the Oman mountains obduction complex. This stage also corresponds to the onset of deposition in the Amiran flexural basin, where the oldest dated sediments were deposited about 82.5–76 Ma (Campanian; *Saura et al.* [2011], and Movie S1 in the supporting information of that article). Deposition is also expected to occur on the NE side of the orogen, toward the open Neo-Tethys domain.

During the Paleocene to Early Eocene stage (Figure 6c) the stacking of the cover thrust sheets of the Kermanshah Complex, when the Zagros Mountains building occurred, is associated with erosion and deposition which are both toward the NE and SW. This stage corresponds to the main development of the Amiran flexural basin (Figure 4). The effects of early growth have not been modeled. At some point, between this stage and the previous, the basement of the Bisotun block started to be emplaced on the hinterland of the Kermanshah complex. This entails the closure of the Harsin basin and the subsequent underthrusting of the Arabian basement beneath the Bisotun basement. The oldest sediments dated in the Gaveh Rud domain correspond to this stage [*Braud*, 1987], recording the onset of subduction of the Neo-Tethys lithosphere

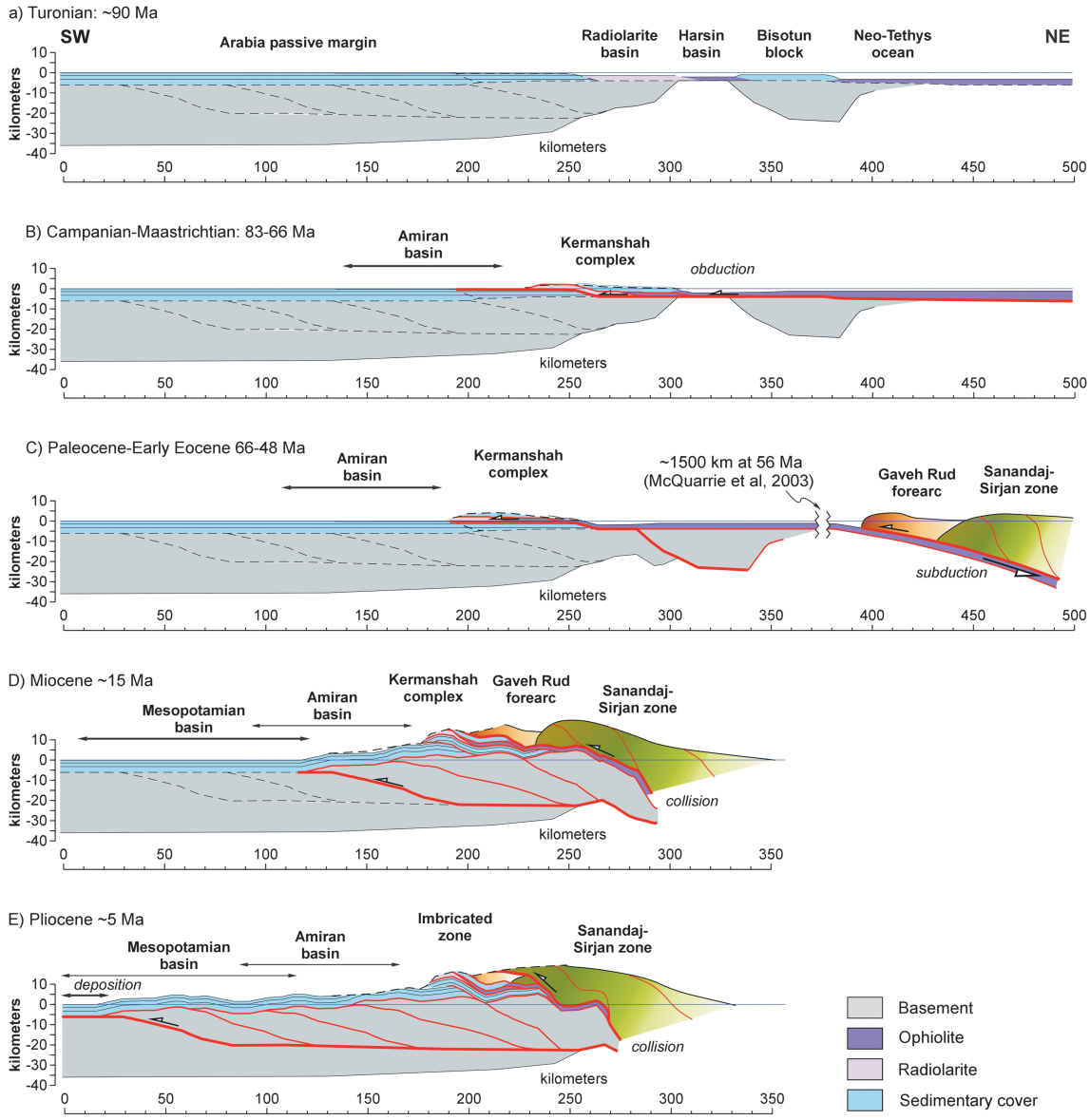

Figure 6. Kinematic model constrained by field data showing the evolution of the Zagros Mountains across the Lurestan area. The SW part of the section, mainly corresponding to the Arabian margin, illustrates the results of the kinematic forward model, without reproducing lithospheric flexure. The NE part, corresponding to the Gaveh Rud volcanic arc and the Sanandaj-Sirjan zone are only qualitatively represented. (a) Initial model at ~90 Ma. (b) Accretion of the Kermanshah complex on top of the Arabian Margin. Onset of deposition in the Amiran basin. (c) Emplacement of the Bisotun basement coeval to evolving subduction below the Sanandaj-Sirjan zone in the northern boundary of the Neo-Tethys ocean. (d) Collision of Arabia and Eurasia and propagation of the shortening along a basement duplex. (e) Final emplacement of the basement duplex along the Mountain Front Fault and associated uplift of the Simply Folded Belt.

beneath this unit. At about 56 Ma, the subduction trench was located ~1500 km NE of the Arabian margin (Figure 6c) [*McQuarrie et al.*, 2003].

The following stage, from late Eocene to early Miocene, corresponds to a period of quiescence, whose onset can be correlated with the deposition of the shallow water Shahbazan Formation, fossilizing the Amiran basin at ~34 Ma (Figure 5). During this stage, the Gaveh Rud domain continued its emplacement on top of the Arabian Margin and reached its final position on top of the Kermanshah complex (Figure 3). During this process, the final closure of the Neo-Tethys Ocean took place and was followed by the onset of the collisional stage. Based on obduction overlap, *McQuarrie and Van Hinsbergen* [2013] propose that this occurred at about 28–27 Ma. Since we propose a shorter overlap, onset of collision in our model is to be expected not earlier than 25–26 Ma.

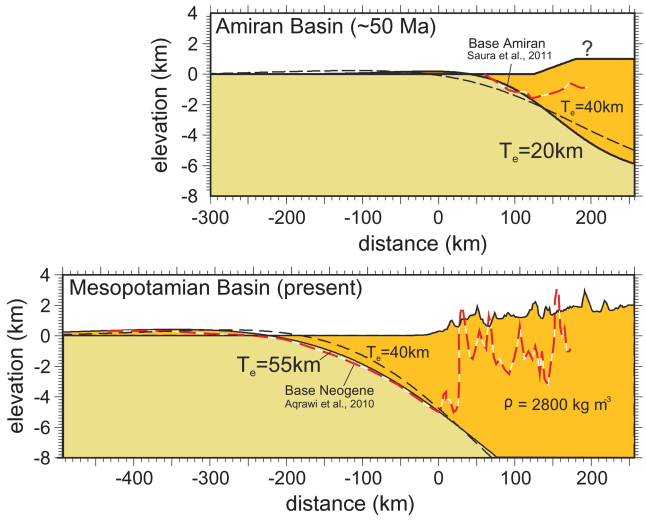

Figure 7. Static flexural profiles calculated for the Amiran and the Mesopotamian stages. The dashed red and white lines indicate observed basin depth (base of the foreland basin subsidence). Bold lines show the best fit model. The result for *Te* = 40 km is shown in each panel for comparison. The different width of the Amiran and Mesopotamian basins can only be reproduced with markedly different lithospheric elastic thicknesses of ~ 20 and 55 km, respectively.

From Miocene to Quaternary (Figures 6d and 6e), the basement of the Arabian margin deformed underneath the decoupled cover units. The emplacement of the basement units was in a piggyback sequence, associated with the out-of-sequence emplacement of the Sanandaj-Sirjan zone in the hinterland. The last stages of the kinematic model (Figure 6e) correspond to the final uplift of the Lurestan area, associated with the major development of the Mesopotamian foreland basin toward the SW (Figure 5).

4. Static Flexural Model: Estimation of Elastic Thickness

The present depth of the Mesopotamian basement and the reconstruction of the Amiran basin thickness allow for a preliminary estimation of the elastic thickness at both stages, which is important to understand the mechanical behavior of the Arabian plate under external forces (tectonic or gravitational). For this purpose, a pure elastic thin plate model is used to calculate the regional isostatic response of the lithosphere under the weight of the Zagros Mountains. Here we fix the final topography and invert the flexural basin depth that isostatically compensates it. To solve the flexural equations, we use an updated version of tAo software [*Garcia-Castellanos et al*., 1997]. It is well established that the vertical motions of a flexural plate submitted to vertical forces are governed by its elastic thickness (*Te*) [*Watts*, 2001]. To convert from flexural rigidity to elastic thickness, Young's modulus and Poisson's ratio of $7 \cdot 10^{10}$ N/m^2 and 0.25, respectively, have been used.

For the Amiran stage, we modify *Te* to search for the best match between the calculated flexural profile and the depth of the basement of the Amiran basin. The Amiran foreland basin is a fossilized flexural basin which has undergone some deformation after its formation. The correlation at 23 Ma presented by *Saura et al*. [2011] using the Asmari Formation horizontal datum grants the best approximation to the geometry of the foreland basin at the end of the obduction stage at about 50 Ma, since major differential vertical movements are not expected within the Amiran basin between 50 and 23 Ma. At 50 Ma the Amiran basin was practically full and presented a structural step in the basement, imaged by the differential depth of the Amiran basin (Figure 4). Taking this into account, the part of the Amiran basin we are trying to fit with the flexural model, is that located ahead of this step in the basement, which would correspond to the geometry of the basin at 50 Ma (Figure 4). Since we lack constraints on the elevation of the topographic load at the time, we assume a 1 km topography, based on the structural step in the inner part of the Amiran basin (Figure 4), associated with the emplacement of the Kermanshah complex in the innermost domains of the chain. The mean density needed to quantitatively explain the basin thickness is 2800 kg/m^3 (see Figure 7), a relatively high value. The

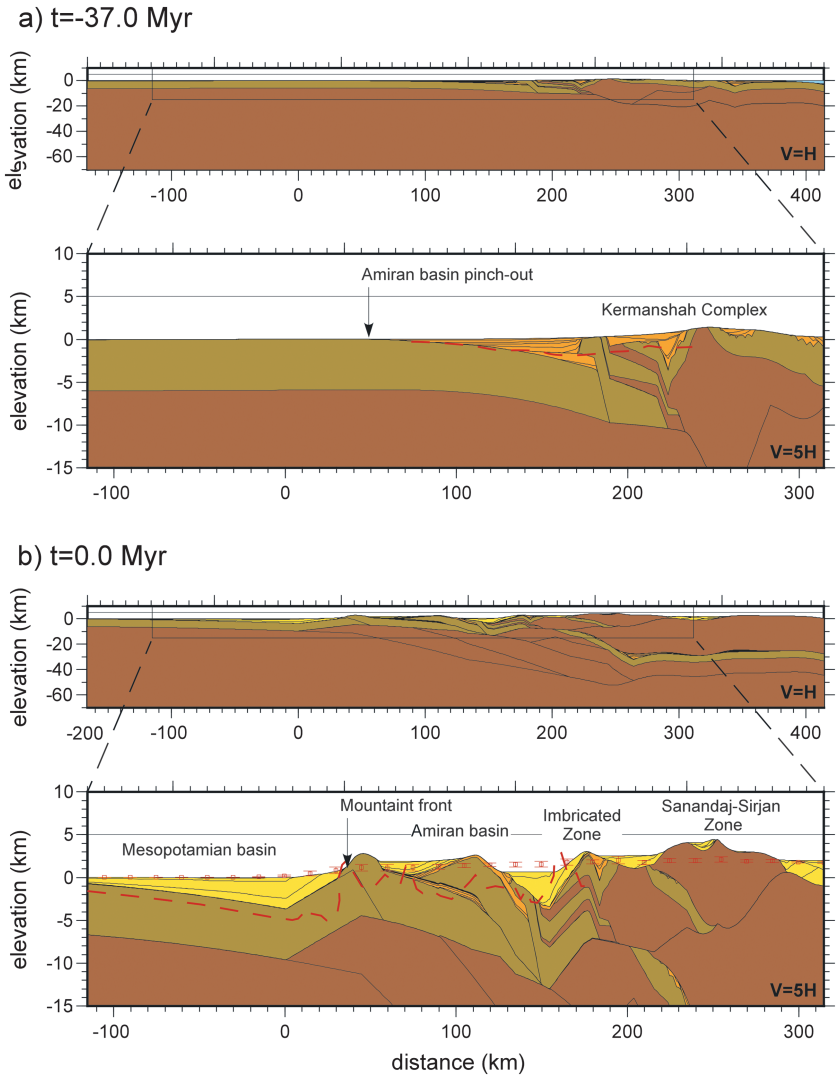

Figure 8. (a) Geometry of the numerical model at −37 Myr, corresponding to the Amiran basin before the onset of collision. (b) Final geometry of the numerical model, corresponding to the present. Sediment horizons every 5 Myr, shade color indicates precollision (orange) and postcollision (yellow). Vertical exaggeration in lower panel is 5X. Note that despite the density of the thrusting units being overestimated in this model (Table 1), the calculated subsidence is insufficient to match the depth of the basement in the Mesopotamian basin.

minor occurrence of tectonic slices with high-density rocks (peridotite and gabbro) within the deformed sedimentary cover in the Imbricated Zone could be a reason for this slight deviation from average densities of sedimentary rocks. The best fit between the flexural profile and the Amiran section is obtained for a *Te* value of 20 km (Figure 7), but acceptable results are obtained within a range of 15–30 km.

We proceed in a similar manner for the Mesopotamian stage. In this case, we use the 18 Ma horizon by *Aqrawi et al.* [2010] as the base of the foreland basin since it is the first horizon that clearly thickens toward the orogen. The best fit is obtained by using an elastic thickness of 55 km (Figure 7), but acceptable results are obtained within a range of 45–70 km.

These results imply a different flexural behavior for both basins, in terms of lithospheric elastic thickness, increasing from about 20 km in the distal parts of the Arabian margin to ~ 55 km under the present Mesopotamian basin. However, the method does not provide information on whether this different behavior of both basins is due to inherited spatial heterogeneities, to temporal changes in lithospheric rigidity, or both.

Table 1. Velocities, Densities, and Timing of the Different Units Used in the Geodynamic Model

Unit	Structural Domain	Horizontal Velocity (km/Myr)	Density (kg/m^3)	Onset of Displacement (Ma)	End of Displacement (Ma)
1	Bisotun cover	−3.5	2600	−90	−80
2	Harsin basin/Bisotun basement	−4.5	2890	−80	−70
3	Radiolarite basin	−4.5	2600	−70	−60
4	Arabian cover 1	−1	2600	−60	−49
5	Eurasia	−11	2890	−35	−20
6	Arabian basement 1	−4	2890	−20	−11
7	Arabian cover 2	−2	2600	−20	−9
8	Arabian basement 2	−4	2890	−11	0
9	Arabian cover 3	−1	2600	−9	0

5. Evolutionary tAo Model: Tectonic, Isostasy, and Surface Transport Evolution

For the evolutionary tAo model (Figure 8), we use the same 2-D (cross section) software, as in the previous section, but here the flexural loads are calculated as a response to the motion of tectonic units with a predefined geometry and velocity. The evolving topography resulting from the motion of these units and their isostatic compensation is eroded by a surface process model. A more exhaustive description is provided in *Garcia-Castellanos* [2007]. The initial model geometry is taken from the restored cross section by *Vergés et al*. [2011b] and the sequence of emplacement, age, and velocities of the model units (Table 1) are based on the kinematic forward model (Figure 6). The density of each unit used to convert motions into load distribution changes is listed in Table 1. For the flexural calculations, we use the *Te* estimates obtained in the previous section. The output model is expected to fit present-day topography and sediment volume, which will add robustness to the geometric model presented by *Vergés et al*. [2011b].

Erosion and sediment transport is calculated as a function of water discharge at each node of the surface. Water is assumed to flow downslope forming lakes in local topographic minima where evaporation is taken into account. Erosion is proportional to the collected water discharge and the local slope at each location, following a stream power law. We use the undercapacity model, as described in *van der Beek and Bishop* [2003], with erosion proportional to the difference between the equilibrium transport capacity and the actual sediment load of the river. Water discharge is calculated from a constant precipitation rate of 500 mm/yr, and constant evaporation rate of 1800 mm/yr is adopted. This can trigger the formation of endorheic basins within the deformed area, if the catchment area of a lake is not large enough to overcome evaporation and allow the lake to overtop. The model parameterization is to some point arbitrary, because of the limitations imposed by the 2-D approach where we lack good constraints on the paleoclimate of the region for the whole modeled period and ignore how much of the precipitation did actually reach the drainage network and participate in eroding the landscape. Since we also lack erodability constraints, we tested different erodability and precipitation values with the only purpose of matching the total cross-sectional area of erosion (estimated from the balanced and restored cross sections) and sediment (obtained from seismic and field data). For the purpose of this study, the key requirement is that the surface transport model roughly reproduces the sediment volumes constrained from the section restoration. The used precipitation and evaporation parameters, with erosion rate much larger than precipitation rate, fall within the range of semiarid to arid climates, which is in agreement with paleoclimate conditions since Late Eocene times which have been proposed for Iran [*Davoudzadeh et al*., 1997; *Ballato et al*., 2008; *Khadivi et al*., 2012].

Modeling results reproduce the main characteristics of the Amiran foreland basin from −83 to −48 Myr, with a width of 140 km and maximum sediment thickness of 2.2 km (Figure 8a). The topography evolution of the hinterland remains below 2 km altitude, reaching its maximum in the early stages and then progressively flattening by erosion. The vertical deflection under the Imbricate Zone reaches 5 km during the last stages of thrust sheet emplacement. Sedimentation continues for ~12 Myr after the end of the obduction-related tectonic processes, prograding outward to complete the basin fill. A 2-D conservative erosion/sedimentation budget is enough to fill this first flexural basin with an average sedimentation rate of 45 m/Myr, in agreement with the restricted nature of the Amiran basin, transversally filled with sediments eroded from the adjacent Imbricated Zone [*Saura et al*., 2011].

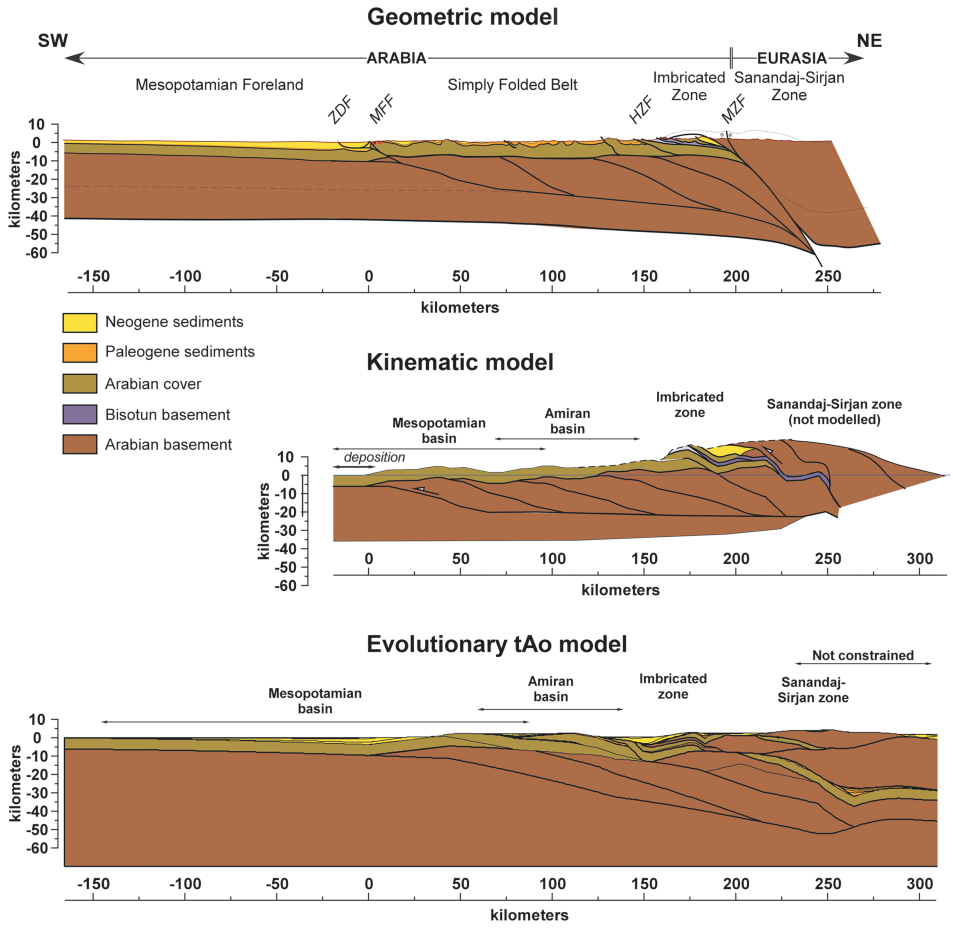

Figure 9. Comparison of the three models presented in this work. Despite evident differences in their final geometry, quantitative comparison of several parameters of the geometric, kinematic, and numerical models (Table 2) provides insights in the understanding of the evolution of the Zagros Mountains.

The Mesopotamian foreland basin is also reproduced by modeling results after −23 Myr, under the load of the Sanandaj-Sirjan zone and the thick basement unit below the obduction complex and the Simply Folded Belt (Figure 8b). However, a 2-D conservative model (i.e., with sediment flow solely along the modeling plane) only accounts for 40% of the sediments currently observed in the Mesopotamian wedge. Based on the current axial drainage network and associated sediment income in the Mesopotamian foreland basin, an additional sedimentation rate of up to 200 m/Myr is introduced into the model, accounting for 60% of the sediments in the basin. This also allows sedimentation to keep pace with subsidence, always remaining above sea level as is the case in the Mesopotamian foreland basin.

The loading of the Iranian plate on top of the Arabian lithosphere together with the imbrication of the basement below the Simply Folded Belt are identified as the main process responsible for the vertical deflection of the Arabian lithosphere below the Imbricated zone, with a maximum of about 10 km and maximum depth and width of the foreland basin of 4 km and 200 km, respectively.

6. Comparison Between the Geometric, Kinematic, and Evolutionary tAo Models

Significant differences arise in the final geometry of the constructed geometric, kinematic, and evolutionary tAo models along the same transect of NW Zagros in Iran (Figure 9). However, these differences are mostly related to the varying initial boundary conditions used for each model, which are mainly conditioned by the modeling method. The geometric model is based on a cross section by *Vergés et al.* [2011b], modified according to geological and geophysical data from different sources

Table 2. Comparison of Geometric Results Between the Geometric, the Kinematic, and the Evolutionary tAo Models

	Geometric Model (km)	Kinematic Model (km)	Evol. tAo Model (km)
Simply Folded Belt width	195	202	191
Imbricated Zone width	56	62	63
Mesopotamian foreland basin width	300	-	200
Mesopotamian foreland basin depth	5	3	4
Maximum crustal thickness	56	38 (54)	57
Maximum detachment depth	60	23 (36)	52
Maximum topography	3.5	16.5	4.4
Final shortening	180	172	182

[*Mohammed*, 2006; *Morley et al*., 2009; *Aqrawi et al*., 2010; *Jiménez-Munt et al*., 2012]. Of the presented models, this is the closest to the actual geometry of the Arabia-Eurasia collision zone. The kinematic model is a forward model aiming to establish the thrust sequence that reproduces the best fit with the geometric model, which would provide insights on the kinematic evolution of the Lurestan area, whereas the evolutionary tAo model is a forward model aimed to fit the observed topography and sediment budget in order to better understand the geodynamic behavior of the area during the orogenic evolution. This required granting realistic and consistent intermediate stages, which further required a simplification exercise. The main similarities and differences between the different models and their implications are discussed below.

6.1. Basin Geometry

Deformation in the Arabian cover of the Simply Folded Belt is mostly characterized by detachment folding and subsidiary thrusting [e.g., *Sattarzadeh et al*., 2000; *Sherkati et al*., 2005; *Vergés et al*., 2011a]. This deformation style is included in the geometric model, although folding of the cover has not been included in the Kinematic model. Besides, detached cover deformation in the Simply Folded Belt is represented by two thrust sheets in the evolutionary tAo model. The geometry of the basement duplex is also different from one model to the other. These are the best fit geometries to reproduce a homogeneous uplift of the Simply Folded Belt, as observed in nature.

The kinematic model does not reproduce flexure, erosion, or sedimentation. This results in a higher topographic profile north of the deformation front and, especially in the innermost parts of the belt, where tectonic stacking is the highest. Erosion has been manually implemented using the present erosion level of each unit as constrain. Sedimentation is not manually added, although the hypothetic location of the foreland basins is indicated (Figures 6 and 9).

Some geometric parameters of the different models can be quantitatively compared (Table 2). The three models show similar widths of the Simply Folded Belt (191–202 km) and the Imbricated Zone (56–63 km). The Mesopotamian foreland basin is 100 km narrower (33%) and 1 km shallower (25%) in the evolutionary tAo model than in the geometric model. This basin is not included in the kinematic model, although the structural step associated with the Mountain Front fault implies 3 km of thickness of the basin fill, 40% less than the geometric model. The geometric and the evolutionary tAo models also present very similar maximum crustal thicknesses (56 and 57 km, respectively), and the maximum crustal thickness of kinematic model measured using the same points as in the geometric model is 54 km which is also very similar to the other models. The maximum depth of the midcrustal detachment is very variable from one model to the other. The geometric model, with a maximum depth of 60 km, supplies the highest value. Instead, the kinematic model with a depth of 23 km supplies the shallowest detachment, but this is mainly due to the Arabian plate remaining unflexed in this model. A simple correction adding the excess topography to the detachment depth, with respect to the geometric model (Table 2), supplies a value of 36 km which is still much below the geometric model. The evolutionary tAo model presents a maximum depth of the midcrustal detachment at 52 km which is also shallower than the geometric model. Final shortening values from the deformation front to the caudal part of the Bisotun thrust sheet are also very similar in the three models (172–182 km).

The final subsidence curve, implicit in the geometric model and the one resulting from the evolutionary tAo model, show very similar trends (Figure 10). These curves overlap from the Zagros deformation front (ZDF) to

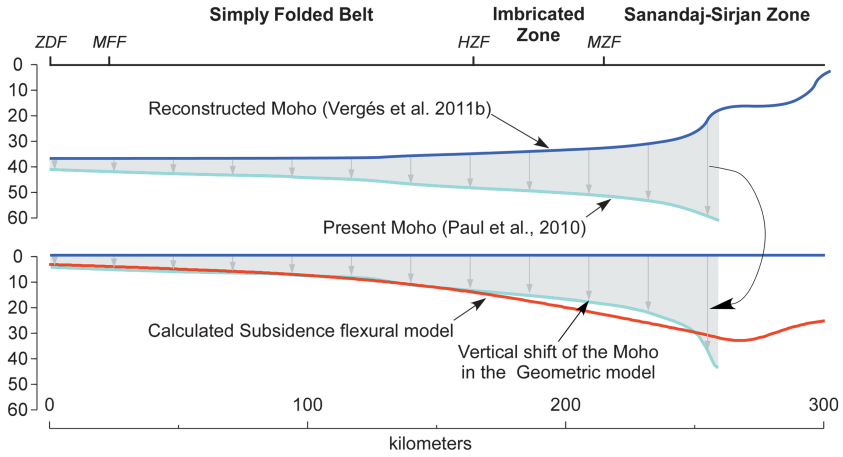

Figure 10. Subsidence curves resulting from the flexural numerical model in this work and from subtracting the current (cyan line) and restored (blue line) geometries of the Moho, according to *Vergés et al.* [2011b] and *Paul et al.* [2010]. ZDF: Zagros deformation front, MFF: Mountain Front fault, HZF: High Zagros fault, MZF: Main Zagros fault. The curves present a good match SW of the High Zagros fault, where the Amiran and Mesopotamian basins are located.

the High Zagros fault (HZF). North of this point, the subsidence is higher in the evolutionary tAo model, although this trend is inverted again below the Imbricated Zone.

6.2. Erosion and Sediment Balance (Cross-Sectional Area of Erosion and Deposition)

Comparison of the balanced and restored cross sections by *Vergés et al.* [2011b] allows us to calculate the final amount of eroded material for each unit in the Lurestan area (Table 3). Given the used 2-D approach, the estimated values of erosion and sediment volume are given in square kilometers of the cross-sectional area. These values supply an initial estimation that can be used to qualitatively constrain the presented geodynamic model. Most of the Radiolarite basin was eroded (~90%), whereas only about 10% of the Harsin basin was washed out. However, since the width of this unit is unconstrained, this is only a minimum value, which would increase if we considered an originally wider Harsin basin. More than 75% of the Bisotun platform was eroded away. This contrasts with the lack of a significant amount of reworked pebbles of this unit within the Amiran basin sediments, which suggests that most of them could have been transported northeastward into the Neo-Tethys Ocean, as already discussed by *Saura et al.* [2013]. In summary, half of the Kermanshah complex was eroded during the whole collision process, which corresponds to a surface of 127 km^2 on the geometrical model (Table 3). This value is comparable to the 133 km^2 of eroded material, calculated by the evolutionary tAo model in the Kermanshah complex. In the SW part of the section, only a small proportion of the upper part of the Arabian margin was eroded (<5% in the Simply Folded Belt). This corresponds to 55 km^2 of eroded section on the geometric model, which is also very similar to the 49 km^2 calculated by the evolutionary tAo model on the same area (Table 3).

During the obduction stage, a maximum accumulation of 210 km^2 of sediments can be estimated for the Amiran basin, one third of which was eroded during the collisional stage. The maximum accumulation of sediments in the Amiran Basin calculated with the evolutionary tAo model is 171 km^2. Finally, a minimum of 300 km^2 is inferred to have been deposited in the inner part of the Mesopotamian basin during the initial collision stages. About 85% of these sediments were eroded during the uplift of the Simply Folded Belt, associated with the emplacement of basement thrust units. The Tertiary sediments preserved in the Mesopotamian basin add up to 565 km^2, whereas the evolutionary tAo model only fills the basin with 316 km^2 of sediments (Table 4). This difference is consistent with the smaller basin dimensions (Table 2).

Table 3. Initial and Eroded Areas of the Main Units of the Geometric and Numerical Cross Sections Across NW Zagros

Structural Domain	Initial Area (km^2)	Geometric Model Eroded Area (km^2)	Numerical Model Eroded Area (km^2)
Arabian margin cover	3124 (1414)	55	49
Kermanshah Complex	216	127	133

Table 4. Maximum and Final Sediment Accumulations in the Geometric Restoration and the Flexural Numerical Model[a]

	Geometric Model		Numerical Model	
Age of Sediment	Maximum Area (km^2)	Final Area (km^2)	Maximum Area (km^2)	Final Area (km^2)
Paleocene to Oligocene	280	189	-	164
Paleocene to Oligocene (only Amiran Basin, maximum volumes are at ~37 Ma)	210	137	171	67
Miocene to Quaternary (SFB + IZ)	>300	57	-	93
Mesopotamian basin	565	565	316	316
Syn-orogenic sediments		811		573

[a]SFB—Simply Folded Belt; IZ—Imbricated Zone. Values are given in cross-sectional area, consistent with 2-D cross-sectional approach.

7. Discussion: Structural and Flexural Evolution of NW Zagros Mountains

7.1. Kinematic Evolution of NW Zagros Mountains

The presented kinematic forward model shows the emplacement sequence as two main stages. The initial stage, associated with obduction, involves the thin thrust sheets of the Kermanshah complex together with the Bisotun basement. The second stage, associated with collision, corresponds to the emplacement of the basement duplex and associated crustal thickening. The number and geometry of the thrust units have been slightly modified in order to generate a best fit with the observed apparent homogeneous uplift of the Simply Folded Belt. This stage also involves the out-of-sequence emplacement of the Gaveh Rud and the Sanandaj-Sirjan zone in the hinterland, on top of the Kermanshah complex. Although the presented model does not reproduce the detailed geometry of the thrust system and the Tertiary basins (Figure 9), it reproduces the main characteristics of the NW Zagros crustal structure [*Vergés et al*., 2011b]. These authors presented the largest shortening estimation published to date for the Zagros Mountains based on crustal area balancing, with an average shortening rate of ~2.0 mm/yr. However, this value is well below the current plate velocities of the Arabian plate, with respect to a fixed Eurasian plate [*Sella et al*., 2002; *Vernant et al*., 2004] and recently published plate scale reconstructions [*Barrier and Vrielynck*, 2008; *Hatzfeld and Molnar*, 2010], leaving a large amount of unaccounted shortening which should probably be concentrated within the boundaries of the minor blocks located on the SW part of the Eurasian plate (Figure 1).

7.2. Flexural Behavior of the Arabian Plate

The best fit between the constraints imposed by the data and the evolutionary tAo model was obtained by considering lateral variations in plate rigidity and stress fields that range from *Te* values of 55 km under the Mesopotamian basin to values of 20 km under the reconstructed Amiran basin and beyond. The lateral *Te* variation is the key to simultaneously explain the flexural behavior and the deviations in the record of vertical motions in the foreland basin and the infill geometries. This northeastward decrease in plate rigidity is consistent with the *Te* maps obtained by *Pérez-Gussinyé et al*. [2009], based on topography and gravity data. It is also in agreement with *Te* estimations from *Tesauro et al*. [2013], based on global data sets of Moho depth and temperature, particularly with their results adopting a "hard" rheology. *Te* values of 20 km during the obduction stage are in agreement with those calculated in Oman [*Ali and Watts*, 2009]. *Te* values of 55 km under the Mesopotamian basin are in agreement with previously published data [*Snyder and Barazangi*, 1986] and fall within the range of similar scenarios elsewhere [*Watts*, 2001; *Garcia-Castellanos and Cloetingh*, 2011; *Tesauro et al*., 2013; *Watts et al*., 2013]. The changing behavior of the Arabian plate could be explained by the eastward increasing stretching of the Arabian plate related to the Late Paleozoic to early Mesozoic rifting episode preceding the opening of the Neo-Tethys [*Stöcklin*, 1968; *Stampfli and Borel*, 2002]. Additionally, the fit between the flexural profile and the Amiran section obtained for the obduction stage also indicates that a 1 km high plateau during the Amiran stage is a likely scenario, although this would require a more detailed study.

7.3. Flexural Loads and Sediment Balance in the NE Zagros Mountains

The evolutionary tAo model provides a tectonic evolution, quantitatively consistent with the history of the foreland basins, with the regional isostasy model and with a simple scenario for the surface process efficiency. The emplacement of Bisotun basement during the obduction stage supplied the tectonic load granting the flexure of Arabian plate and formation of the Amiran foreland basin. Material eroded from the

imbricated zone during this stage was enough to fill the Amiran basin, as already proposed by *Saura et al*. [2013]. This suggests a transversal drainage system during the Late Cretaceous to Early Eocene.

Flexure of the Arabian plate below the Mesopotamian basin was triggered by the emplacement of basement units under the Simply Folded Belt during the last 20 Myr. However, the maximum subsidence obtained by the geodynamic model was well below that observed in seismic data (Figure 8b). This suggests that an extra load is required to accomplish total flexure of the Arabian plate which is probably related to subcrustal processes. Similar mantle-sourced additional loads have been derived from previous flexural studies in foreland basin settings, such as the Guadalquivir Basin [*García-Castellanos et al*., 2002] and the Sub-Andean Basin [*Dávila et al*., 2007]. Comparing our flexural model (Figure 8) with the Mesopotamian basin architecture of *Aqrawi et al*. [2010] (Figure 5) suggests that this additional subsidence may have taken place during the early stages of Mesopotamian sedimentation (18–12 Ma), since deformation along the frontalmost thrusts started significantly later than that (<10 Ma) [e.g., *Homke et al*., 2004; *Emami et al*., 2010]. The uncertainties in these kinematic constraints of the forefront deformation and in the basin infill geometry call for future independent assessment of this point. *García-Castellanos et al*. [2002] quantified the excess subsidence of the Guadalquivir basin, relative to that expected from the isostatic compensation of the Betic cordillera topography, and related it to the lateral variations of crustal and lithospheric thickness. In contrast, *Dávila et al*. [2005, 2007] link an excess subsidence of the Sub-Andean foreland to dynamic loads, purportedly related to mantle flow. *Garcia-Castellanos and Cloetingh* [2011] summarize other possible mechanisms for foreland basin subsidence different from thrust stacking, such as the pull of a subducted slab, the horizontal compression, and the effects of the developing thrusts on the stress distribution within the bending plate [see also *Simpson*, 2014]. Finally, the 2-D approach also disregards the combined 3-D effect of topography and weight of sediment accumulation.

Additionally, material eroded from the Simply Folded Belt and the Imbricated Zone was not enough to fill the Mesopotamian basin, which required additional sediment supply of 200 m/Myr in the foredeep. In the Mesopotamian basin, this additional supply should be provided by an axial drainage system, which can be correlated by the influx of paleo-Tigris and paleo-Eufrates Rivers, transporting sediments from northwesternmost areas [e.g., *Vergés*, 2007]. During the collision stage, two different wedge top basins can be differentiated. The Neogene basins located more to the south correspond to the innermost parts of the Mesopotamian foreland basin, uplifted and eroded during the latest stages of collision, after −15 Myr. The youngest sediments filling these basins are very recent and could be correlated with the youngest sediments in the Lurestan domain [*James and Wynd*, 1965; *Emami*, 2008; *Pirouz et al*., 2011]. On the other hand, a small basin forms between the Imbricated and the Sanandaj-Sirjan zones, which is thrusted southwestward to be finally emplaced on top of the Imbricated Zone (Figure 8b). During the emplacement of this basin it is partially eroded and feeds younger basins forelandward. This basin could be correlated with the Gaveh Rud domain, a fore-arc basin developed in front of the Sanandaj-Sirjan zone. Erosion and resedimentation of Gaveh Rud basin fill could explain the Middle to Late Eocene exhumation stage recorded in the Agha Jari formation in the foreland basin [*Homke et al*., 2010].

7.4. Implications of the Evolutionary tAo Model in the Understanding of the Innermost Zagros Domains

The thrust system depicted in the geometric model implies a very efficient basement cover decoupling, along which the Sanandaj-Sirjan zone emplaced on top of the Kermanshah complex, transmitted a portion of the collision-related shortening to the Zagros belt cover (Figure 9). This decoupling surface was rooted at depth along the Main Zagros Fault, the Arabia-Eurasia suture. Notwithstanding, the evolutionary tAo model required a NE directed thrust fault to step up and breach the surface, about 160 km NE of the High Zagros Fault. This double verging structural configuration of the entire collision zone (Figure 2) agrees with the NE verging fault system bounding thick Neogene sedimentary basins in the Central Basin region in Iran, according to *Morley et al*. [2009] and *Ballato et al*. [2011].

The evolutionary tAo model shows the distal segment of the Arabian plate, including the Neo-Tethys domain, subducted below Eurasia (Figure 8b). The rather flat resultant of the Eurasia-Arabia contact is a consequence of the used code not differentiating crust and mantle, although a similar model based on receiver functions was proposed for this transect by *Paul et al*. [2010] and *Hatzfeld and Molnar* [2010]. This

model would imply a relatively flat subduction with more than 200 km of overthrusting between the Sanandaj-Sirjan Zone and the Neo-Tethys oceanic domain. Nonetheless, seismic tomography profiles show a contrasting subvertical change in mantle velocities coinciding with the Arabia-Eurasia suture at surface [*Vergés et al*., 2011b] and thus implying a steep contact between the Arabia and Iran plates at depth, as proposed by *Vergés et al*. [2011b]. Therefore, the results of the evolutionary tAo model depicted the portion of the Arabian plate that should sink into the mantle during Neogene times. This subducted subvertical oceanic lithosphere beneath the inner part of the Zagros Belt could be the source for the hidden load required by the evolutionary tAo model to fit the depth and wavelength of the modeled Mesopotamian foreland basin (Figure 8b).

8. Conclusions

The comparison of the presented geometric, kinematic, and evolutionary models demonstrates that the geometric model proposed for the Arabia-Eurasia collision along NE Iranian Zagros, implying a shortening of ~180 km, well above most shortening estimations in the area, is a plausible scenario. The restored geometry of the Arabian Margin combined with plate reconstructions of the area [*McQuarrie and Van Hinsbergen*, 2013] allows us to propose that onset of collision is to be expected not earlier than 25–26 Ma.

The kinematic forward model confirms a thrust emplacement sequence in two major stages, the first involving the Bisotun basement and the Kermanshah complex cover thrust sheets. The second stage corresponds to the duplexing of the basement thrust units, the deformation of the Arabian cover in the Simply Folded Belt, and the out-of-sequence emplacement of Gaveh Rud and Sanandaj-Sirjan Zone in the hinterland. Deformation in the basement seems to be less localized than initially proposed, and therefore, the number and geometry of the thrust units have been slightly modified in order to generate a better fit with the observed apparently homogeneous uplift of the Simply Folded Belt.

Variation in time and space of the elastic thickness of the Arabian plate is needed in order to fit the different geometries of the Amiran and Mesopotamian foreland basins. According to elastic thin plate modeling, the elastic thickness increased from about 20 km in the distal parts of the Arabian margin during the Late Cretaceous and Paleocene to ~ 55 km under the present Mesopotamian basin during Miocene and Pliocene times.

The results of the evolutionary tAo model show that the proposed sequence and timing of thrust emplacement during the obduction phase generate a foreland basin whose dimensions are comparable to the Amiran basin at 41 Ma. Emplacement of Bisotun basement during this stage is fundamental to the supply of the required load. Similarly, the emplacement sequence during the collision phase generates a foreland basin that is comparable to the present Mesopotamian basin, although ~100 km narrower and ~1 km shallower. The bulk of this flexural basin is formed in response to the emplacement of basement units during the last 10 Myr. However, an extra load which is coeval to this process is required to explain about 20% of the Arabian plate flexure. This hidden load could be related to the proposed hanging steep Neo-Tethys slab beneath the inner Zagros Belt.

The evolutionary tAo model of tectonic, topographic, and surface transport evolution shows that erosion of the Kermanshah complex during the obduction stage supplied enough sediment to fill the Amiran basin. In contrast, the sediment supplied by the Zagros uplift during the collision stage was not sufficient to fill the Mesopotamian flexural foreland, which required an additional sediment supply of up to 200 m/Myr. This additional deposition could be supplied by the axial income of the paleo-Tigris and paleo-Euphrates Rivers from elevated regions to the north and northeast (Anatolian and Iranian plateaus).

Acknowledgments
This research was carried out with the aid of grants by CSIC-FSE 2007–2013 JAE-Doc postdoctoral research contract (E.S.) and with funding from the Spanish Research Agency through project Tecla (CGL2011-26670). We thank DARIUS Programme for their additional support. The paper benefitted from the thoughtful comments by two anonymous reviewers. All structural geological data presented in this paper can be obtained from the lead author. The tAo software can be downloaded from https://sites.google.com/site/daniggcc/software/tao.

References

Abdollahie Fard, I., A. Braathen, M. Mokhtari, and S. A. Alavi (2006), Interaction of the Zagros Fold-Thrust Belt and the Arabian type, deep-seated folds in the Abadan Plain and the Dezful Embayment, SW Iran, *Petrol. Geosci.*, *12*, 347–362.

Agard, P., J. Omrani, J. Jolivet, and F. Mouthereau (2005), Convergence history across Zagros (Iran): Constraints from collisional and earlier deformation, *Int. J. Earth Sci. (Geol Rundsch)*, *94*, 401–419.

Agard, P., J. Omrani, L. Jolivet, H. Whitechurch, B. Vrielynck, W. Spakman, P. Monié, B. Meyer, and R. Wortel (2011), Zagros orogeny: A subduction-dominated process, *Geol. Mag.*, *148*(5–6), 692–725.

Alavi, M. (2004), Regional stratigraphy of the Zagros fold-thrust belt of Iran and its proforeland evolution, *Am. J. Sci.*, *304*, 1–20.

Alavi, M. (2007), Structures of the Zagros fold-thrust belt in Iran, *Am. J. Sci.*, *307*, 1064–1095, doi:10.2475/09.2007.02.

Ali, M. Y., and A. B. Watts (2009), Subsidence history, gravity anomalies and flexure of the United Arab Emirates (UAE) foreland basin, *GeoArabia*, *14*(2), 17–44.
Alsharhan, A. S. (1989), Petroleum geology of the United Arab Emirates, *J. Pet. Geol.*, *12*(3), 253–288.
Aqrawi, A. A. M., J. C. Goff, A. Horbury, and F. N. Sadooni (2010), *The Petroleum Geology of Iraq*, 424 pp., Scientific Press, Great Britain.
Babaie, H. A., A. Babaei, A. M. Ghazi, and M. Arvin (2006), Geochemical, 40Ar/39Ar age, and isotopic data for crustal rocks of the Neyriz ophiolite, Iran, *Can. J. Earth Sci.*, *43*(1), 57–70.
Ballato, P., N. R. Nowaczyk, A. Landgraf, M. R. Strecker, A. Friedrich, and S. H. Tabatabaei (2008), Tectonic control on sedimentary facies pattern and sediment accumulation rates in the Miocene foreland basin of the southern Alborz mountains, northern Iran, *Tectonics*, *27*, TC6001, doi:10.1029/2008TC002278.
Ballato, P., C. E. Uba, A. Landgraf, M. R. Strecker, M. Sudo, D. F. Stockli, A. Friedrich, and S. H. Tabatabaei (2011), Arabia-Eurasia continental collision: Insights from late Tertiary foreland-basin evolution in the Alborz Mountains. Northern Iran, *Bull. Geol. Soc. Am.*, *123*(1–2), 106–131.
Ballato, P., D. F. Stockli, M. Ghassemi, A. Landgraf, M. R. Strecker, J. Hassanzadeh, A. Friedrich, and S. H. Tabatabaei (2013), Accommodation of transpressional strain in the Arabia-Eurasia collision zone: New constraints from (U-Th)/He thermochronology in the Alborz mountains, N Iran, *Tectonics*, *32*, 1–18, doi:10.1029/2012TC003159.
Barrier, E., and B. Vrielynck, (Contributors: Bergerat, F., Brunet, M.-F., Mosar, J., Poisson, A. & Sosson, M.) (2008), *Palaeotectonic Maps of the Middle East: Tectonono-Sedimentary-Palinspastic Maps From Late Norian to Pliocene*, CGMW, Paris, France, Atlas of 14 maps at 1/18 500 000.
Berberian, M. (1995), Master "blind" thrust faults hidden under the Zagros folds: Active basement tectonics and surface morphotectonics, *Tectonophysics*, *241*, 193–224.
Berberian, M., and G. C. P. King (1981), Towards a paleogeography and tectonic evolution of Iran, *Can. J. Earth Sci.*, *18*, 210–265.
Blanc, E. J.-P., M. B. Allen, S. Inger, and H. Hassani (2003), Structural styles in the Zagros Simple Folded Zone, Iran, *J. Geol. Soc., London*, *160*, 401–412.
Braud, J. (1987), La suture du Zagros au niveau de Kermanshah (Kurdistan Iranien): Reconstitution paléogéographique, évolution géodynamique, magmatique et structurale, PhD thesis, 450 pp., Univ. Paris-Sud, Orsay, France.
Casciello, E., J. Vergés, E. Saura, G. Casini, N. Fernández, E. Blanc, S. Homke, and D. Hunt (2009), Fold patterns and multilayer rheology of the Lurestan Province, Zagros Simply Folded Belt (Iran), *Geol. Soc. London*, *166*, 947–959, doi:10.1144/0016-76492008-76492138.
Dávila, F. M., R. A. Astini, and T. E. Jordan (2005), Subcrustal loads in the Andean foreland and pampean plain: Stratigraphic, topographic and geophysical evidence, Cargas subcorticales en el antepaís andino y la planicie pampeana: Evidencias estratigráficas, topográficas y geofísicas, *Rev. Asoc. Geol. Argent.*, *60*(4), 775–786.
Dávila, F. M., R. A. Astini, T. E. Jordan, G. Gehrels, and M. Ezpeleta (2007), Miocene forebulge development previous to broken foreland partitioning in the southern Central Andes, west-central Argentina, *Tectonics*, *26*, TC5016, doi:10.1029/2007TC002118.
Davoudzadeh, M., B. Lammerer, and K. Weber-Diefenbach (1997), Paleogeography, stratigraphy, and tectonics of the tertiary of Iran, *Neues Jahrbuch fur Geologie und Palaontologie—Abhandlungen*, *205*(1), 33–67.
Delaloye, M., and J. Desmons (1980), Ophiolites and melange terranes in Iran: A geochronological study and its paleotectonic implications, *Tectonophysics*, *68*(1–2), 83–111.
Dunnington, H. V. (1968), Salt-tectonic features of northern Iraq, in *Saline Deposits: A Symposium Based on Papers From the International Conference on Saline Deposits*, edited by R. B. Mattox, *Geol. Soc. Am. Spec. Pap.*, *88*, 183–227.
Emami, H. (2008), Foreland propagation folding and structure of the Mountain Front Flexure in the Pusht-e Kuh arc (NW Zagros, Iran), PhD thesis, 181 pp., Univ. de Barcelona, Barcelona, Spain.
Emami, H., J. Vergés, T. Nalpas, P. Gillespie, I. Sharp, R. Karpuz, E. P. Blanc, and M. G. H. Goodarzi (2010), Structure of the Mountain Front Flexure along the Anaran anticline in the Pusht-e Kuh Arc (NW Zagros, Iran): Insights from sand box models, *Geol. Soc. London, Spec. Publ.*, *330*, 155–178.
Fakhari, M. D., G. J. Axen, B. K. Horton, J. Hassanzadeh, and A. Amini (2008), Revised age of proximal deposits in the Zagros foreland basin and implications for Cenozoic evolution of the High Zagros, *Tectonophysics*, *451*(1–4), 170–185.
Farzipour-Saein, A., A. Yassaghi, S. Sherkati, and H. Koyi (2009), Basin evolution of the Lurestan region in the Zagros fold-and-thrust belt, Iran, *J. Pet. Geol.*, *32*(1), 5–19.
Fouad, S. (2010), Tectonic and structural evolution of the Mesopotamia foredeep, Iraq, *Geosurviraq*, *6*(2), 41–53.
Garcia-Castellanos, D. (2007), The role of climate during high plateau formation. Insights from numerical experiments, *Earth Planet. Sci. Lett.*, *257*(3–4), 372–390.
Garcia-Castellanos, D., and S. Cloetingh (2011), Modeling the interaction between lithospheric and surface processes in foreland basins, in *Tectonics of Sedimentary Basins: Recent Advances*, edited by C. Busby and A. Azor, pp. 152–181, John Wiley, Chichester, U. K., doi:10.1002/9781444347166.ch8.
Garcia-Castellanos, D., M. Fernàndez, and M. Torne (1997), Numerical modeling of foreland basin formation: A program relating thrusting, flexure, sediment geometry and lithospehre rheology, *Comput. Geosci.*, *23*(9), 993–1003.
García-Castellanos, D., M. Fernández, and M. Torne (2002), Modeling the evolution of the Guadalquivir foreland basin (southern Spain), *Tectonics*, *21*(3), 1041, doi:10.1029/2002TC001339.
Gavillot, Y. G., G. Axen, D. F. Stockli, B. K. Horton, and M. Fakhari (2010), Timing of thrust activity in the High Zagros fold-thrust belt, Iran, from (U-Th)/He thermochronometry, *Tectonics*, *29*, TC4025, doi:10.1029/2009TC002484.
Glennie, K. W., M. G. A. Boeuf, M. W. Hughes Clarke, M. Moody-Stuart, W. F. H. Pilaar, and B. M. Reinhardt (1974), *Geology of the Oman Mountains: Verhandelingen van het Koninklijk Nederlands Geologisch Mijnbouwkundig Genootschap*, 423 pp., Den Haag, Koninklijk Nederlands Geologisch Mijnbouwkundig Genootschap, Nederlands.
Gök, R., H. Mahdi, H. Al-Shukri, and A. J. Rodgers (2008), Crustal structure of Iraq from receiver functions and surface wave dispersion: Implications for understanding the deformation history of the Arabian-Eurasian collision, *Geophys. J. Int.*, *172*(3), 1179–1187.
Golonka, J. (2004), Plate tectonic evolution of the southern margin of Eurasia in the Mesozoic and Cenozoic, *Tectonophysics*, *381*, 235–273.
Hatzfeld, D., and P. Molnar (2010), Comparisons of the kinematics and deep structures of the Zagros and Himalaya and of the Iranian and Tibetan plateaus and geodynamic implications, *Rev. Geophys.*, *48*, RG2005, doi:10.1029/2009RG000304.
Hessami, K., H. A. Koyi, C. J. Talbot, H. Tabasi, and E. Shabanian (2001), Progressive unconformities within an evolving foreland fold-and-thrust belt, Zagros Mountains, *Geol. Soc. London*, *158*, 969–981.
Homke, S., J. Vergés, M. Garcés, H. Emami, and R. Karpuz (2004), Magnetostratigraphy of Miocene–Pliocene Zagros foreland deposits in the front of the Push-e Kush Arc (Lurestan Province, Iran), *Earth Planet. Sci. Lett.*, *225*, 397–410.
Homke, S., J. Vergés, J. Serra-Kiel, G. Bernaola, I. Sharp, M. Garcés, I. Montero-Verdú, R. Karpuz, and M. H. Goodarzi (2009), Late Cretaceous-Paleocene formation of the proto-Zagros foreland basin, Lurestan Province, SW Iran, *Geol. Soc. Am. Bull.*, *121*(7/8), 963–978, doi:10.1130/B26035.26031.

Homke, S., J. Vergés, P. Van der Beek, M. Fernàndez, E. Saura, L. Barbero, B. Badics, and E. Labrin (2010), Insights in the exhumation history of the NW Zagros from bedrock and detrital apatite fission-track analysis: Evidence for a long-lived orogeny, *Basin Res.*, *22*, 659–680, doi:10.1111/j.1365-2117.2009.00431.x.

Horton, B. K., J. Hassanzadeh, D. F. Stockli, G. J. Axen, R. J. Gillis, B. Guest, A. Amini, M. D. Fakhari, S. M. Zamanzadeh, and M. Grove (2008), Detrital zircon provenance of Neoproterozoic to Cenozoic deposits in Iran: Implications for chronostratigraphy and collisional tectonics, *Tectonophysics*, *451*(1–4), 97–122.

James, G. A., and J. G. Wynd (1965), Stratigraphic nomenclature of Iranian oil consortium agreement area, *Bull. Am. Assoc. Petrol. Geol.*, *49*(12), 2182–2245.

Jassim, S. Z., and J. C. Goff (2006), *Geology of Iraq*, 341 pp., Dolin, Prague and Moravian Museum, Brno.

Jiménez-Munt, I., M. Fernàndez, E. Saura, J. Vergés, and D. Garcia-Castellanos (2012), 3-D lithospheric structure and regional/residual Bouguer anomalies in the Arabia-Eurasia collision (Iran), *Geophys. J. Int.*, *190*(3), 1311–1324.

Karim, K. H., H. Koyi, M. M. Baziany, and K. Hessami (2011), Significance of angular unconformities between Cretaceous and Tertiary strata in the northwestern segment of the Zagros fold–thrust belt, Kurdistan Region, NE Iraq, *Geol. Mag.*, *148*(5–6), 925–939.

Khadivi, S., F. Mouthereau, J. C. Larrasoaña, J. Vergés, O. Lacombe, E. Khademi, E. Beamud, M. Melinte-Dobrinescu, and J. P. Suc (2010), Magnetochronology of synorogenic Miocene foreland sediments in the Fars arc of the Zagros Folded Belt (SE Iran), *Basin Res.*, *22*, 918–932, doi:10.1111/j.1365-2117.2009.00446.x.

Khadivi, S., F. Mouthereau, J. Barbarand, T. Adatte, and O. Lacombe (2012), Constraints on palaeodrainage evolution induced by uplift and exhumation on the southern flank of the Zagros-Iranian plateau, *J. Geol. Soc.*, *169*(1), 83–97.

Lawa, F. A., H. Koyi, and A. Ibrahim (2013), Tectono-stratigraphic evolution of the NW segment of the Zagros fold-thrust belt, Kurdistan, NE Iraq, *J. Pet. Geol.*, *36*(1), 75–96.

McQuarrie, N. (2004), Crustal scale geometry of the Zagros fold–thrust belt, Iran, *J. Struct. Geol.*, *26*, 519–535.

McQuarrie, N., and D. J. Van Hinsbergen (2013), Retrodeforming the Arabia-Eurasia collision zone: Age of collision versus magnitude of continental subduction, *Geology*, *41*(3), 315–318.

McQuarrie, N., J. M. Stock, C. Verdel, and B. P. Wernicke (2003), Cenozoic evolution of Neotethys and implications for the causes of plate motions, *Geophys. Res. Lett.*, *30*(20), 2036, doi:10.1029/2003GL017992.

Mohammed, S. A. G. (2006), Megaseismic section across the northeastern slope of the Arabian Plate, Iraq, *GeoArabia*, *11*(4), 77–90.

Molinaro, M., J. C. Guezou, P. Leturmy, S. A. Eshraghi, and D. Frizon de Lamotte (2004), The origin of changes in structural style across the Bandar Abbas syntaxis, SE Zagros (Iran), *Mar. Pet. Geol.*, *21*, 735–752.

Molinaro, M., P. Leturmy, J.-C. Guezou, D. Frizon de Lamotte, and S. A. Eshraghi (2005), The structure and kinematics of the south-eastern Zagros fold thrust belt; Iran: From thin-skinned to thick-skinned tectonics, *Tectonics*, *24*, TC3007, doi:10.1029/2004TC001633.

Morley, C. K., B. Kongwung, A. A. Julapour, M. Abdolghafourian, M. Hajian, D. Waples, J. Warren, H. Otterdoom, K. Srisuriyon, and H. Kazemi (2009), Structural development of a major late Cenozoic basin and transpressional belt in central Iran: The Central Basin in the Qom-Saveh area, *Geosphere*, *5*(4), 325–362.

Motiei, H. (1993), Stratigraphy of Zagros, in *Treatise on the Geology of Iran*, *Geol. Surv. Iran*, vol. 1, pp. 281–289, Geol. Surv. of Iran Rep., Tehran.

Mouthereau, F., O. Lacombe, and B. Meyer (2006), The Zagros folded belt (Fars, Iran): Constraints from topography and critical wedge modelling, *Geophys. J. Int.*, *165*, 336–356.

Mouthereau, F., J. Tensi, N. Bellahsen, O. Lacombe, T. de Boisgrollier, and S. Kargar (2007), Tertiary sequence of deformation in a thin-skinned/thick-skinned collision belt: The Zagros Folded Belt (Fars, Iran), *Tectonics*, *26*, TC5006, doi:10.1029/2007TC002098.

Mouthereau, F., O. Lacombe, and J. Vergés (2012), Building the Zagros collisional orogen: Timing, strain distribution and the dynamics of Arabia/Eurasia plate convergence, *Tectonophysics*, *532–535*, 27–60.

Nolan, S. C., P. W. Skelton, B. P. Clissold, and J. D. Smewing (1990), Maastrichtian to early Tertiary stratigraphy and palaeogeography of the Central and Northern Oman Mountains, *Geol. Soc. London Spec. Publ.*, *49*(1), 495–519.

Paul, A., D. Hatzfeld, A. Kaviani, M. Tatar, and C. Pequegnat (2010), Seismic imaging of the lithospheric structure of the Zagros mountain belt (Iran), *Geol. Soc. London Spec. Publ.*, *330*(1), 5–18.

Pérez-Gussinyé, M., M. Metois, M. Fernandez, J. Vergés, J. Fullea, and A. Lowry (2009), Effective elastic thickness of Africa and its relationship to other proxies for lithospheric structure and surface tectonics, *Earth Planet. Sci. Lett.*, *287*, 152–167, doi:10.1016/j.epsl.2009.1008.1004.

Pirouz, M., G. Simpson, A. Bahroudi, and A. Azhdari (2011), Neogene sediments and modern depositional environments of the Zagros foreland basin system, *Geol. Mag.*, *148*(5–6), 838–853.

Piryaei, A., J. J. G. Reijmer, F. S. P. V. Buchem, M. Yazdi-Moghadam, J. A. Piryaei, J. J. G. Reijmer, F. S. P. V. Buchem, and M. Yazdi-Moghadam (2010), The influence of Late Cretaceous tectonic processes on sedimentation patterns along the northeastern Arabian plate margin (Fars Province, SW Iran), *Geol. Soc. London Spec. Publ.*, *330*, 211–251, doi:10.1144/SP330.11.

Robertson, A. H. F., M. P. Searle, and A. C. Ries (1990), *The Geology and Tectonics of the Oman Region*, edited by K. Coe, *Geol. Soc. London Spec. Publ.*, *49*, 835.

Ruh, J. B., A. M. Hirt, J.-P. Burg, and A. Mohammadi (2014), Forward propagation of the Zagros Simply Folded Belt constrained from magnetostratigraphy of growth strata, *Tectonics*, *33*, 1534–1551, doi:10.1002/2013TC003465.

Saccani, E., K. Allahyari, L. Beccaluva, and G. Bianchini (2013), Geochemistry and petrology of the Kermanshah ophiolites (Iran): Implication for the interaction between passive rifting, oceanic accretion, and OIB-type components in the Southern Neo-Tethys Ocean, *Gondwana Res.*, *24*(1), 392–411.

Sattarzadeh, Y., J. W. Cosgrove, and C. Vita-Finzi (2000), The interplay of faulting and folding during the evolution of the Zagros deformation belt, in *Forced Folds and Fractures*, vol. 169, edited by J. W. Cosgrove and M. S. Ameen, pp. 187–196, Geol. Soc. of London, London.

Saura, E., et al. (2011), Basin architecture and growth folding of the NW Zagros early foreland basin during the Late Cretaceous and early Tertiary, *J. Geol. Soc.*, *168*(1), 235–250.

Saura, E., J. C. Embry, J. Vergés, D. W. Hunt, E. Casciello, and S. Homke (2013), Growth fold controls on carbonate distribution in mixed foreland basins: Insights from the Amiran foreland basin (NW Zagros, Iran) and stratigraphic numerical modelling, *Basin Res.*, *25*, 149–171.

Searle, M. P., et al. (1987), The closing of Tethys and the tectonics of the Himalaya, *Bull. Geol. Soc. Am.*, *98*, 678–701.

Sella, G., T. H. Dixon, and A. Mao (2002), REVEL: A model for recent plate velocities from space geodesy, *J. Geophys. Res.*, *107*(4), 2081–2111, doi:10.1029/2000JB000033.

Sengor, A. M. C. (1990), A new model for the late Palaeozoic–Mesozoic tectonic evolution of Iran and implications for Oman, *Geol. Soc. London Spec. Publ.*, *49*(1), 797–831.

Sherkati, S., and J. Letouzey (2004), Variation of structural style and basin evolution in the central Zagros (Izeh zone and Dezful Embayment), Iran, *Mar. Pet. Geol.*, *21*(5), 535–554.

Sherkati, S., M. Molinaro, D. Frizon de Lamotte, and J. Letouzey (2005), Detachment folding in the Central and Eastern Zagros fold-belt (Iran): Salt mobility, multiple detachments and late basement control, *J. Struct. Geol.*, *27*, 1680–1696, doi:10.1016/j.jsg.2005.1605.1010.

Simpson, G. (2014), Decoupling of foreland basin subsidence from topography linked to faulting and erosion, *Geology*, *42*(9), 775–778.

Snyder, D. B., and M. Barazangi (1986), Deep crustal structure and flexure of the Arabian plate beneath the Zagros collisional mountain belt as inferred from gravity observation, *Tectonics*, *5*(3), 361–373, doi:10.1029/TC005i003p00361.

Stampfli, G. M., and G. D. Borel (2002), A plate tectonic model for the Paleozoic and Mesozoic constrained by dynamic plate boundaries and restored synthetic oceanic isochrons, *Earth Planet. Sci. Lett.*, *196*, 17–33.

Stöcklin, J. (1968), Structural history and tectonics of Iran: A review, *Am. Assoc. Pet. Geol. Bull.*, *52*, 1229–1258.

Stoneley, R. (1981), The geology of the Kuh-e Dalneshim area of southern Iran, and its bearing on the evolution of southernTethys, *J. Geol. Soc. London*, *138*, 509–526.

Talbot, C. J., and M. Alavi (1996), The past of a future syntaxis across the Zagros, in *Salt Tectonics*, vol. 100, edited by G. I. Alsop, D. J. Blundell, and I. Davison, pp. 89–109, Geol. Soc. of London, London.

Talebian, M., and J. Jackson (2004), A reappraisal of earthquake focal mechanisms and active shortening in the Zagros mountains of Iran, *Geophys. J. Int.*, *156*(3), 506–526.

Tatar, M., D. Hatzfeld, and M. Ghafori-Ashtiany (2004), Tectonics of the Central Zagros (Iran) deduced from microearthquake seismicity, *Geophys. J. Int.*, *156*, 255–266.

Tesauro, M., M. K. Kaban, and S. A. P. L. Cloetingh (2013), Global model for the lithospheric strength and effective elastic thickness, *Tectonophysics*, *602*, 78–86.

van der Beek, P., and P. Bishop (2003), Cenozoic river profile development in the Upper Lachlan catchment (SE Australia) as a test of quantitative fluvial incision models, *J. Geophys. Res.*, *108*(B6), 2309, doi:10.1029/2002JB002125.

Vergés, J. (2007), Drainage responses to oblique and lateral thrust ramps: A review, in *Sedimentary Processes, Environments and Basins: A Tribute to Peter Friend*, chap. 3, edited by G. Nichols, C. Paola, and E. Williams, *Int. Assoc. Sedimentol. Spec. Publ.*, *38*, 29–47, doi:10.1002/9781444304411.ch3.

Vergés, J., M. H. Goodarzi, H. Emami, R. Karpuz, J. Efstatiou, and P. Gillespie (2011a), Multiple detachment folding in Pusht-e Kuh Arc, Zagros. Role of mechanical stratigraphy, in *Thrust Fault Related Folding*, edited by K. McClay, J. Shaw, and J. Suppe, *Mem. AAPG*, *94*, 1–26, doi:10.1306/13251333M942899.

Vergés, J., E. Saura, E. Casciello, M. Fernàndez, A. Villaseñor, I. Jiménez-Munt, and D. Garcia-Castellanos (2011b), Crustal-scale cross-sections across the NW Zagros belt: Implications for the Arabian margin reconstruction, *Geol. Mag.*, *148*(5–6), 739–761, doi:10.1017/S0016756811000331.

Vernant, P., et al. (2004), Present-day crustal deformation and plate kinematics in the Middle Est constrained by GPS measurements in Iran and northern Oman, *Geophys. J. Int.*, *157*, 381–398.

Warburton, J., T. J. Burnhill, R. H. Graham, and K. P. Isaac (1990), The evolution of the Oman Mountains Foreland Basin, *Geol. Soc. London Spec. Publ.*, *49*(1), 419–427.

Watts, A. B. (2001), *Isostasy and Flexure of the Lithosphere*, vol. 458, Cambridge Univ. Press, Cambridge, U. K.

Watts, A. B., S. J. Zhong, and J. Hunter (2013), The behavior of the lithosphere on seismic to geologic timescales, *Annu. Rev. Earth Planet. Sci.*, *41*, 443–468.

Wrobel-Daveau, J.-C., J.-C. Ringenbach, S. Tavakoli, G. Ruiz, P. Masse, and D. Frizon de Lamotte (2010), Evidence for mantle exhumation along the Arabian margin in the Zagros (Kermanshah area, Iran), *Arabian J. Geosci.*, *3*(4), 499–513.